Distribution, chemical and molecular composition of high and low-molecular-weight humic-like substances in ambient aerosols

Xingjun Fan[a,b,*], Ao Cheng[a], Xufang Yu[a], Tao Cao[b,c], Dan Chen[a], Wenchao Ji[a], Yongbing Cai[a], Fande Meng[a], Jianzhong Song[b,**], Ping'an Peng[b]

[a] College of Resource and Environment, Anhui Science and Technology University, Fengyang 233100, P. R. China

[b] State Key Laboratory of Organic Geochemistry, Guangzhou Institute of Geochemistry, Chinese Academy of Sciences, Guangzhou 510640, P. R. China

[c] University of Chinese Academy of Sciences, Beijing, 100049, PR China

* Corresponding authors

E-mail addresses: fanxj@ahstu.edu.cn (Xingjun Fan), songjzh@gig.ac.cn (Jianzhong Song)

Abstract

18   Humic-like Substances (HULIS) encompass a continuum of molecular weight

19 (MW) ranges, yet our understanding of how HULIS characteristics vary with MW is

20 still limited and not well-established. In this study, a combination of ultrafiltration and

21 solid-phase extraction protocols was employed to fractionate the high MW (HMW, >1

22 kDa) and low MW (LMW, < 1kDa) HULIS fractions from ambient aerosols collected

23 during summer and winter at a rural site. Subsequently, comprehensive

24 characterization by using total organic carbon, high-performance size exclusion

25 chromatography (HPSEC), UV-vis and fluorescence spectroscopy, Fourier-transform

26 infrared spectroscopy (FTIR), negative electrospray ionization high resolution mass

27 spectrometry (ESI- HRMS) were conducted. The results revealed that HMW HULIS

28 were dominated by larger-sized chromophores, substantially constituting a higher

29 fraction of total organic carbon and UV absorption at 254 nm than LMW HULIS.

30 While both HMW and LMW HULIS shared similar fluorophore types and functional

31 groups, the former exhibited higher levels of humification and a greater presence of

32 polar functional groups (e.g., -COOH, >C=O). HRMS analysis further unveiled that

33 molecular formulas within HMW HULIS generally featured smaller sizes but higher

34 degrees of unsaturation and aromaticity compared to those within LMW HULIS

35 fractions. This observation suggests the possibility of small molecules assembling to

36 form the HMW HULIS through intermolecular weak forces. Moreover, HMW HULIS

37 contained a higher proportion of CHON but fewer CHO compounds than LMW

38 HULIS. In both HMW and LMW HULIS, the unique molecular formulas were

39 primarily characterized by lignin-like species, yet the former displayed a prevalence

40 of N-enriched and highly aromatic species. Additionally, HMW HULIS contained

41 more unique lipids-like compounds, while LMW HULIS exhibited a distinct presence

42 of tannin-like compounds. These findings provide valuable insights into the

43 distribution, optical properties, and molecular-level characteristics of HULIS in

44 atmospheric aerosols, thereby advancing our understanding of their sources,

45 composition, and environmental implications.

46

47 **Keywords:** Humic-Like Substances, molecular weight fractionation, optical

48 properties, high-performance size exclusion chromatography, negative electrospray

49 ionization-high resolution mass spectrometry

50

1. Introduction

HUmic-Like Substances (HULIS) are complex and heterogeneous mixtures of water-soluble organic matters (WSOM) that are of great importance in the atmospheric environment. They usually share similar physicochemical properties (e.g., acidity, absorption, fluorescence, functional groups) with naturally occurring humic substances (Graber and Rudich, 2006; Zheng et al., 2013) and are prevalent in fog, clouds, rainwater and ambient aerosols (Birdwell and Valsaraj, 2010; Fan et al., 2016a; Santos et al., 2012). With substantial hygroscopic and surface-active properties, HULIS enhance the hygroscopic growth of particles, thereby contributing to the formation of the cloud condensation nuclei and ice nuclei (Chen et al., 2021a; Dinar et al., 2007). Moreover, acting as an important component of brown carbon (BrC), HULIS effectively absorb near-ultraviolet and visible light, thus influencing the global radiative balance and atmospheric chemistry processes (Bao et al., 2022; Zhang et al., 2020). Furthermore, HULIS have the potential to catalyze the formation of reactive oxygen species, leading to potential adverse health effects (Ma et al., 2019; Zhang et al., 2022b).

The chemical composition of atmospheric HULIS exhibit significant heterogeneity and typically comprises macromolecular compounds containing aromatic rings with highly conjugated structures, as well as long-chain hydrocarbon with polar groups (e.g., -OH, -COOH, $-NO_2$) (Fan et al., 2013; Huo et al., 2021). To unravel the structural characteristics and properties of HULIS, a range of analytical techniques, including absorption and fluorescence spectroscopy, Fourier transform

infrared spectroscopy (FTIR), nuclear magnetic resonance spectroscopy (^{1}H NMR), have been utilized (Huo et al., 2021; Qin et al., 2022; Zou et al., 2020). These studies have provided insights into the overall structural characteristics of complex HULIS, including their abundances, chemical and optical characteristics (Huo et al., 2021; Mukherjee et al., 2020; Win et al., 2018; Zhang et al., 2022b; Zheng et al., 2013). In recent years, high-resolution mass spectrometry (HRMS) techniques, such as Fourier transform ion cyclotron resonance mass spectrometry (FT-ICR-MS) and orbitrap HRMS, in combination with electrospray ionization (ESI), have emerged as powerful tools for elucidating the molecular-level characteristics of HULIS (Lin et al., 2012; Sun et al., 2021; Wang et al., 2019; Zou et al., 2023). By utilizing HRMS, researchers have gained deeper insights into the complexity and chemical heterogeneity of HULIS at the molecular level.

Operationally, HULIS are defined as the hydrophobic fraction of water-soluble organic matter (WSOM) typically extracted through solid-phase extraction (SPE) protocol (Fan et al., 2012; Zou et al., 2020). Thus, the abundance and characteristics of HULIS are contingent upon the chemical composition of WSOM. Previous studies have shown that aerosol WSOM, often seen as water-soluble brown carbon (BrC), are comprised of a continuum of molecular weight (MW) species, as revealed by high-performance exclusion chromatography (HPSEC) analysis (Di Lorenzo et al., 2017; Fan et al., 2023; Wong et al., 2019). These studies have highlighted that BrC typically consist of both high-MW (HMW) and low-MW (LMW) chromophores in various aerosols. For example, BrC emitted from fresh biomass burning (BB) are

95   dominated by low MW chromophores (Di Lorenzo et al., 2017; Wong et al., 2019).

96   However, BrC derived from aged BB aerosols and ambient aerosols tend to possess

97   more HMW chromophores that are highly chemically resistant (Di Lorenzo et al.,

98   2017; Fan et al., 2023; Wong et al., 2019). Further characterizations of different MW

99   BrC can be conducted using an ultrafiltration (UF) protocol (Fan et al., 2021). This

100   approach enabled researchers to obtain the distributions of content, chromophores and

101   fluorophores within various MW BrC fractions. Despite these advancements, the

102   chemical structures and molecular composition of different MW HULIS fractions

103   remain poorly understood. Consequently, a combination of UF and SPE protocols for

104   the fractionation and characterization of MW-separated HULIS is crucial, as it not

105   only provides insights into MW distributions but also illuminates the chemical

106   heterogeneities of aerosols HULIS.

107   In this study, a combination of UF-SPE isolation protocol was developed to

108   fractionate and characterize the MW HULIS fractions. Two distinct sets of ambient

109   $PM_{2.5}$ samples collected during summer and winter periods were utilized to facilitate a

110   comparative analysis of MW HULIS. Initially, the WSOM were fractionated into

111   high-MW (HMW, >1 kDa) and low-MW (LMW, <1 kDa) species using the UF

112   protocol. Subsequently, the resulting MW WSOM fractions underwent SPE to obtain

113   different MW HULIS fractions. The obtained HMW and LMW HULIS fractions were

114   comprehensively characterized using advanced analytical techniques, including total

115   organic carbon analysis, UV-vis and fluorescence spectroscopy, HPSEC, and HRMS

116   to unveil their abundances, absorption and fluorescence properties, and molecular

characteristics. The findings of this study hold great significance in advancing our understanding of the definition and molecular profiles of HULIS, as well as facilitating further investigations into their potential impacts on the atmospheric environment.

2. Materials and methods

2.1. Atmospheric fine particles sampling

Atmospheric $PM_{2.5}$ were sampled on the rooftop of a building within the campus of Anhui Science and Technology University (32.21ºN, 118.72ºE), around 20 m above ground level. Detailed information regarding the sampling site can be found in our previous studies (Cao et al., 2022; Fan et al., 2021). The $PM_{2.5}$ samples were collected using a high-volume $PM_{2.5}$ sampler (JCH-1000, Juchuang Ltd., Qingdao) onto prebaked quartz fiber filters (8 × 10 inches, Whatman). Sampling took place from July 25 to August 12, 2021, during summer, and from December 19, 2021 to January 6, 2022, during winter. Blank filters were also collected as control samples. All aerosol $PM_{2.5}$ filter samples were stored at -20 ºC in a freezer prior to analysis. The atmospheric pollutant data (NO_2, SO_2 and O_3) near sampling site during sampling period were obtained from the website (https://www.aqistudy.cn) and are summarized in Table S1. Additionally, the fire spots were investigated using data from the website (https://firms.modaps.eosdis.nasa.gov/map/) and are visualized in Fig. S1.

2.2. Application of UF-SPE for isolating MW HULIS fractions

139   Punches of summer and winter aerosol $PM_{2.5}$ filter samples were taken and

140   combined for the extraction of water-soluble organic matter (WSOM), respectively.

141   The filters were immersed in 300 mL of ultrapure water and subjected to

142   ultrasonication for 30 min. The resulting suspensions were then filtered through a 0.22

143   μm membrane (Φ 47 mm, Jinteng, China) to obtain bulk WSOM samples. These bulk

144   filtrates were further subjected to UF and SPE in tandem to obtain different MW

145   HULIS fractions. Please refer to Fig. S2 for a schematic representation of the

146   fractionation steps.

147   Before UF, the bulk WSOM were diluted to DOC concentration below 30 mg/L

148   to minimize the concentration effects and prevent the accumulation of organic matters

149   at the membrane surface during UF. The detailed UF procedure followed the profile

150   described in our previous study (Fan et al., 2021). Briefly, each bulk WSOM solution

151   was passed through a pre-cleaned 1 kDa cut-off membrane in a stirred UF cell

152   (Amicon 8200, Millipore, USA), with a pressure at 0.2 MPa applied by ultrapure N_2.

153   The concentration factor was ~10. The resulting retentate was considered as HMW

154   (>1 kDa) WSOM, while the permeate solutions represented the LMW (<1 kDa)

155   WSOM. Finally, each MW fraction was diluted to the initial volume for further

156   treatment and analysis. Mass balances of WSOM during one-step UF process

157   generally ranged from 92% to 99%, as determined by total organic carbon (TOC) and

158   UV absorption at 254 nm (UV_{254}), indicating good performance of UF without

159   substantial loss or organic contamination.

160   Subsequently, SPE was applied to isolate the so-called HULIS fractions from the

161 bulk and each MW fraction of WSOM, following the protocol proposed in our

162 previous studies (Fan et al., 2013; Zou et al., 2020). Briefly, the acidified aqueous

163 samples were passed through pre-activated HLB columns (Waters Oasis, 500 mg/6

164 mL, USA). The fractions retained on the resins (referred to as HULIS) were eluted

165 with pure methanol and dried using a gentle stream of pure N_2. Finally, the bulk,

166 HMW and LMW HULIS fractions were obtained. A blank filter control was

167 performed using the same procedure described above, and the analysis signals of

168 samples were corrected by blank control.

169

170 2.3. HPSEC analysis

171   The apparent MW distributions of MW HULIS fractions were analyzed using a

172 high-performance liquid chromatography (HPLC) system (LC-20AT, Shimadzu,

173 Japan) equipped with a refractive index detector (RID-10A, Shimadzu) and a diode

174 array detector (SPD-M20A, Shimadzu). The wavelength of the diode array detector

175 was set at 254 nm. Separation was performed using an aqueous gel filtration column

176 (Polysep-GFC-P 3000, Phenomenex) preceded by a guard column (Polysep-GFC-P,

177 Phenomenex). The mobile phase consisted of a mixture of water and methanol (90:10

178 v/v) containing 25 mM ammonium acetate (Di Lorenzo et al., 2017; Wong et al.,

179 2019). The sample injection volume was 100 μL, and the flow rate was maintained at

180 1 mL min^{-1}. The HPSEC calibration was performed using a series of polyethylene

181 glycol (PEG) standards (Kawasaki et al., 2011; Zhang et al., 2022c). The

182 chromatographic peak areas were integrated to represent the abundances of

corresponding MW species. It should be noted that the MW values estimated here are nominal rather than absolute due to the lack of appropriate standards for column calibration (Fan et al., 2023; Wong et al., 2017).

The weight-average MW (Mw), number-average MW (Mn) and polydispersivity (ρ), were determined using the following equations (Song et al., 2010):

$$Mw = \frac{\sum_{i=1}^{n} (h_i MW_i)}{\sum_{i=1}^{n} h_i} \qquad (1)$$

$$Mn = \frac{\sum_{i=1}^{n} h_i}{\sum_{i=1}^{n} (h_i/MW_i)} \qquad (2)$$

$$\rho = \frac{Mw}{Mn} \qquad (3)$$

where h_i and MW_i are the absorption intensity of the chromatogram and the MW of molecules corresponding to the ith retention time, respectively.

2.4. Measurements of WSOC content and optical properties

The concentration of water-soluble organic carbon (WSOC) in HMW and LMW HULIS was measured using a Shimadzu TOC analyzer (TOC-VCPN, Japan) following the non-purgeable organic carbon protocol.

The UV-vis spectra were recorded using a UV-vis spectrophotometer (UV 2600, Shimadzu, Japan) over a wavelength range of 200-700 nm with 1 nm increments. Excitation-emission matrix (EEM) spectra were determined using a fluorescence spectrophotometer (F4600, Hitachi, Japan). The scanning ranges for excitation (Ex) and emission (Em) wavelengths were 200-400 and 290-520 nm, respectively, with a scanning speed was 12,000 nm/min.

To characterize the chemical and optical properties of MW HULIS fractions,

202 several commonly used spectra parameters were calculated, including the specific UV

203 absorbance at 254 nm ($SUVA_{254}$), the UV absorbance ratio between 250 and 365 nm

204 (E_2/E_3), spectra slope ratios (S_R), the absorption Angstrom exponent (AAE), and mass

205 absorption efficiency (MAE_{365}), fluorescence indices (FI), biological index (BIX), and

206 humification degree (HIX) (Fan et al., 2021; Li et al., 2022; Wu et al., 2021). Further

207 details can be found in Text S1 of the Supporting Information (SI).

208

209 2.5. HRMS analysis and data processing

210 The MW HULIS fractions were analyzed using a Q-Exactive mass spectrometer

211 (Thermo Scientific, Germany) equipped with a heated electrospray ionization (ESI)

212 source. The system operated in negative ESI mode with a resolution of 140,000 at m/z

213 = 200. The detection mass range was set from 60 to 900 m/z. To ensure accurate mass

214 measurements, mass calibration was carried out using a commercial standard mixture

215 of ESI-L Low Concentration Tuning Mix (G1969-85000, Agilent, USA).

216 The acquired mass spectra were processed using Xcalibur software (V2.2,

217 Thermo Scientific). The mathematically possible formulas for all ions were calculated

218 with a signal-to-noise ratio (s/n) $\geq$ 5 using a mass tolerance of 5 ppm. The assigned

219 molecular formulas followed specific constraints, with limitations on the following

220 elements: C $\leq$ 50, H $\leq$ 100, O $\leq$ 20, N $\leq$ 3, S $\leq$ 2. Additionally, the elemental ratios of

221 H/C, O/C, N/ C, and S/C were constrained to the ranges of 0.3–3.0, 0–3.0, 0–0.5, and

222 0–2.0, respectively. The double-bond equivalents (DBE) and modified aromaticity

223 index (AI_{mod}) values of the assigned neutral assigned formula ($C_cH_hO_oN_nS_s$) were

224   calculated using the equations (4-5) (He et al., 2023; Song et al., 2022):

$$\text{DBE} = 1 + \frac{1}{2}(2c - h + n) \tag{4}$$

$$\text{AI}_{mod} = \frac{1 + c - 0.5o - 0.5n - 0.5h}{c - 0.5o - n} \tag{5}$$

225   The intensity-weighted molecular parameters (X_w) of MW, H/C, O/C, DBE, and

226   AI values were calculated according to the equation (6) (He et al., 2023; Zhang et al.,

227   2021; Zou et al., 2023):

$$X_W = \frac{\sum(I_i \cdot X_i)}{\sum I_i} \tag{6}$$

228   where X represents the aforementioned parameters, and I_i denote the intensity for each

229   assigned formula i.

230

231   **3. Results and discussion**

232   3.1. Size and distribution of MW HULIS fractions

233   3.1.1. Molecular size of HMW and LMW HULIS

234   Fig. 1 shows the HPSEC chromatograms of MW HULIS. Both HMW and LMW

235   HULIS exhibit MW continuum distributions ranging from 100 to 20,000 Da, which is

236   consistent with the reported distributions of BrC in BB-derived and various ambient

237   aerosol in previous studies (Di Lorenzo et al., 2017; Fan et al., 2023; Wong et al.,

238   2017). However, the chromatographic patterns for HMW HULIS clearly differ from

239   those observed for LMW HULIS in both aerosol samples. As seen in Fig. 1, HMW

240   HULIS display an additional and stronger absorption peak at around 4000 Da (peak

241   *iii*), along with a more pronounced peak at 2200 Da (peak *ii*) and a similar magnitude

242   peak at 570 Da (peak *i*) compared to LMW HULIS. This suggests that HMW HULIS

243   contain the majority of larger molecular size chromophores within the bulk WSOM.

244   In addition, the magnitude peak at 570 Da (peak i) in HMW HULIS may indicate the

245   incorporation of small molecule through weak interactions based on π–π and/or van

246   der Waals forces between the HULIS components (Fan et al., 2021; Piccolo, 2002).
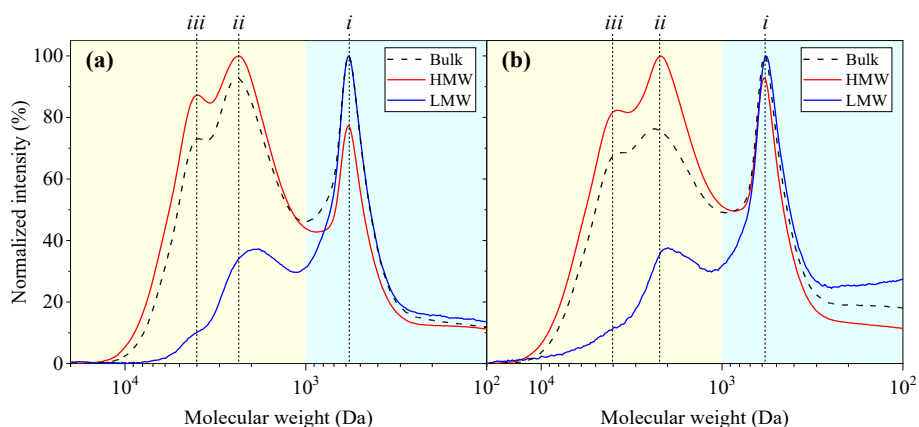
247

248   **Fig. 1.** Average HPSEC chromatograms of bulk, HMW and LMW HULIS fractions in

249   (a) summer and (b) winter aerosol, respectively. The yellow and cyan shadows

250   represent MW size regions of >1 kDa and <1 kDa, respectively.

251

252   Moreover, the molecular size of MW HULIS can be further reflected by the

253   differences in Mw and Mn. As listed in Table 1, the average Mw and Mn of HMW

254   HULIS are 2233-2315 and 654-707 Da, respectively, greatly larger than that of LMW

255   HULIS (989-1071 and 293-394 Da, respectively). These differences indicate that the

256   sources and formation processes of HMW HULIS may differ from LMW HULIS.

257   Many previous studies have demonstrated that fresh BB HULIS generally consist of

258   small molecular-sized chromophores (Di Lorenzo et al., 2018; Di Lorenzo et al., 2017;

259   Wong et al., 2017; Wong et al., 2019). However, a notable enhancement in the

260   formation of large molecular-sized chromophores has been found when they undergo

261   intricate atmospheric processes (Di Lorenzo et al., 2018; Di Lorenzo et al., 2017;

262   Wong et al., 2017; Wong et al., 2019). Based on these limited studies, it is suggested

263   that HMW HULIS, characterized by higher proportions of large-size chromophores

264   and the resulting larger apparent molecular size, might be associated with the products

265   from atmospheric aging process rather than being emitted directly by primary sources.

266

267   **Table 1.** The summary of typical quantity and quality parameters of each MW HULIS

268   fraction from BB and ambient aerosols.

		Summer			Winter		
		Bulk	HMW	LMW	Bulk	HMW	LMW
HPSEC-derived parameters	M_w	1975±13	2315±38	1071±24	1918±56	2233±42	989±67
	M_n	591±53	707±48	394±13	525±57	654±17	293±32
	ρ	3.4±0.3	3.3±0.2	2.7±0.2	3.7±0.3	3.4±0.2	3.4±0.2
HULIS/WSOM (%)[a]	TOC	65±1	68±1	51±2	63±2	67±2	41±1
	UV_{254}	66±5	65±2	55±4	67±1	65±1	61±2
Optical parameters	E_2/E_3	12.02±0.54	11.72±0.31	14.98±0.98	6.30±0.24	6.54±0.16	7.24±0.43
	MAE_{365}	0.21±0.02	0.23±0.01	0.20±0.01	1.04±0.02	1.06±0.01	0.88±0.00
	AAE	7.11±0.32	7.59±0.00	8.25±0.23	6.66±0.06	6.25±0.06	7.28±0.03
	FI	2.00±0.04	1.99±0.03	2.04±0.05	2.06±0.01	1.97±0.03	2.25±0.02
	BIX	0.95±0.01	0.86±0.07	1.02±0.01	0.96±0.01	0.81±0.01	1.07±0.02
	HIX	2.42±0.06	2.43±0.04	2.40±0.05	3.13±0.25	5.64±0.34	1.94±0.16

269   [a] The ratios of contents of SPE-isolated HULIS fractions to that of corresponding

270   WSOM fractions determined by TOC and/or absorbance at 254 nm (UV_{254}).

271

272   3.1.2. Relative abundances of HMW and LMW HULIS

273   The contribution of MW-HULIS fractions to their corresponding MW-WSOM

274   fractions, quantified in terms of TOC and UV absorption at 254 nm for both summer

275   and winter aerosols are summarized in Table 1. In general, the ratios of

276   HULIS/WSOM of HMW fractions (in terms of TOC and UV254) (65-68%) were

higher than the ratios (41-61%) observed for LMW fractions. This finding suggests that the higher presence of hydrophobic and conjugated aromatic structures in HMW WSOM, but more hydrophilic OC and non-aromatic species (e.g., aliphatic dicarboxylic acid) in the LMW WSOM (Fan et al., 2012; Zou et al., 2020).

Fig. 2 illustrates the distribution of distinct MW fractions within reconstructed WSOM, wherein "non-HULIS" refers to the content differences between the MW WSOM and its HULIS fractions. The HMW HULIS fraction contributed 39-41% of TOC and 40-47% of UV254 to the bulk WSOM. In contrast, the LWM HULIS fraction only make up a smaller proportion, accounting for 16-20% of TOC and 17-21% of UV254 within the bulk WSOM. Specifically, the ratios between HMW HULIS and LMW HULIS (H/L) ranged from 1.88 to 2.75 for both summer and winter aerosols in terms of either TOC or UV254. These findings emphasize that HMW HULIS significantly dominate the bulk aerosol HULIS fractions. Notably, the H/L ratio for winter aerosols was higher than that for summer aerosols, suggesting that larger-sized HULIS contributed more to the bulk HULIS fractions in winter aerosols.

292
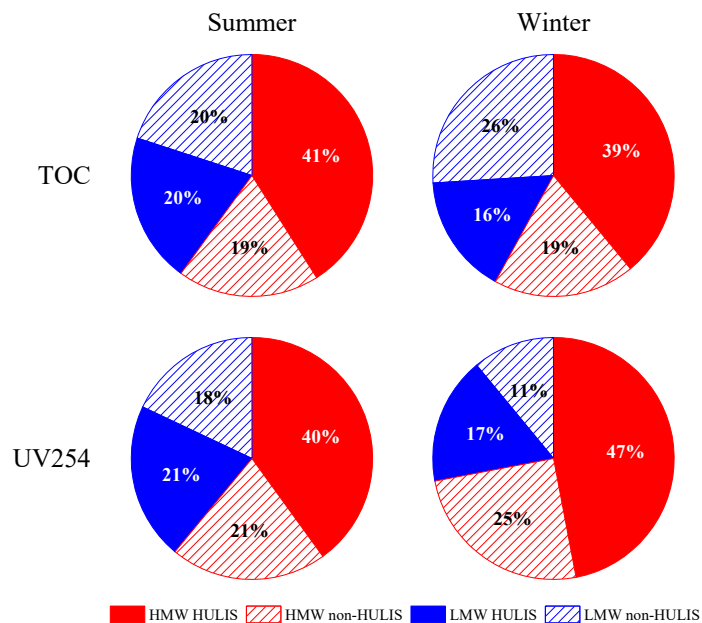
Fig. 2. Relative proportions of different MW fractions in summer and winter aerosols

determined by TOC and UV254.

295

The non-HULIS fractions are also important constituents within aerosol WSOM,

but exhibit some differences between HMW and LMW fractions. The contributions of

HMW non-HULIS to bulk WSOM were ~19% as determined by TOC and 21-25%

measured by UV254. In case of LMW non-HULIS, the contributions were higher in

terms of TOC (20-26%) but lower in terms of UV254 (11-18%). These results

indicate that the LMW WSOM contain a larger proportion of hydrophilic organic

species with weaker light absorption.

303

3.2. Optical characteristics of MW HULIS fractions

3.2.1. Light absorption characteristics

The absorption spectra of MW HULIS fractions in ambient aerosols are shown in

Fig. S3. These spectra exhibit a featureless shape with a general decrease in

absorbance as the wavelength increases, which is a typical characteristic of HULIS

found in rainwater, biomass burning (BB), and ambient aerosols (Huo et al., 2021;

Santos et al., 2009; Zhang et al., 2022b). The E_2/E_3 ratio, commonly used as an

indicator of the chemical characteristics of organic species, is inversely correlated

with higher aromaticity and larger molecular weight (Fan et al., 2021; Li et al., 2022;

Sun et al., 2021). As listed in Table 1, the E_2/E_3 of HMW HULIS fractions generally

were lower than that of LMW HULIS in both ambient aerosols. This is consistent

with the expectation that larger-sized HULIS generally possess more polyconjugated

and polymeric structures (Fan et al., 2021; Zhang et al., 2022c), leading to greater

aromaticity and larger molecular size.

MAE$_{365}$ and AAE are commonly used to characterize the light absorption

capacity and the spectral dependence of light absorption by aerosol chromophores,

respectively (Bao et al., 2022; Fan et al., 2016b; Kumar et al., 2017; Yuan et al., 2021;

Zou et al., 2020). As listed in Table 1, the average MAE$_{365}$ values of HMW HULIS

are 0.23 and 1.06 $m^2\ g^{-1}$ in summer and winter aerosol, respectively. These values are

higher than the corresponding values of 0.20 and 0.88 $m^2\ g^{-1}$, respectively, for LMW

HULIS. In addition, HMW HULIS presented lower AAE values, being 7.59 and 6.25

in summer and winter aerosol, respectively, than the corresponding values of 8.25 and

7.28, respectively, for LMW HULIS (Table 1). These findings are consistent with the

observation in our previous study that larger WSOM generally own higher MAE$_{365}$

but smaller AAE values than smaller WSOM (Fan et al., 2021). Generally, the results

suggest that HMW HULIS exhibit stronger light-absorbing ability but with light

absorption showing a weaker wavelength dependence. It is worth noting that combustion sources, such as BB and coal combustion, usually emit primary HULIS with high MAE_{365} values due to the enrichment of poly-aromatic and unsaturated species (Cao et al., 2021; Fan et al., 2018; Huo et al., 2021; Zhang et al., 2021), but with small molecular weight distributions (Di Lorenzo et al., 2018; Di Lorenzo et al., 2017; Wong et al., 2017). Furthermore, subsequent pronounced photooxidation and photobleaching processes can lead to a enrichment and/or formation of large sized chromophores (Di Lorenzo et al., 2018; Di Lorenzo et al., 2017; Wong et al., 2017), concurrently resulting in a reduction in their absorption capacity and an enhancement of their spectra dependence on wavelength (Chen et al., 2021b; Fan et al., 2019; Wu et al., 2018; Wu et al., 2020; Zhang et al., 2022a). From this perspective, the SOA formation might induce the generation of HMW HULIS with lower light absorption capacity and weaker light absorption wavelength dependence. In contrast, LMW HULIS is more likely to represent small-sized primary HULIS and/or by-products resulting from the degradation and oxidation of primary large-sized HULIS. Considering the complex sources of ambient HULIS, future studies should explore the MW-dependent light absorption characteristics of HULIS from different sources.

3.2.2. Fluorescence characteristics

The EEM contours of MW HULIS fractions from both summer and winter aerosols are presented in Fig. S4. These HULIS fractions from both seasons exhibit similar EEM spectra features, with a predominance of humic-like fluorophores

(Ex/Em = 210-235/395-410 nm). This observation suggest that humic-like fluorophores are fundamental constituents of both HMW and LMW HULIS, which are consistent with previous findings for aerosols MW WSOM (Fan et al., 2021) and bulk HULIS in BB-derived and ambient aerosols (Fan et al., 2020; Qin et al., 2018). The findings imply an assembly of small and heterogeneous molecules to form bulk HULIS through weak intramolecular forces (i.e., π–π, van der Waals, hydrophobic, or hydrogen bonds) (Fan et al., 2021; Piccolo, 2002) and/or charge-transfer interactions (Phillips et al., 2017; Qin et al., 2022). In this study, the fluorescence regional integration (FRI) method was applied to characterize the fluorescent composition of MW HULIS. Using FRI, EEM spectra were divided into five fluorescence regions (labeled as I to V) (Fig. S4), which were successively assigned to simple aromatic proteins (I and II), fulvic acid-like (III), soluble microbial byproduct-like (IV), and humic acid-like (V) substances, respectively, as established in previous studies (Chen et al., 2003; Qin et al., 2018; Wang et al., 2021b). As shown in Fig. S5, the large-size aromatic proteins (II) and fulvic acid-like substances (III) dominated the fluorophores within MW HULIS in both summer and winter aerosols, comprising approximately 62-64% of the total fluorescence intensity. This finding is consistent with previous reports on bulk HULIS in summer and winter aerosols from industrial and urban cities (Qin et al., 2018; Wang et al., 2021b). In comparison, the HMW HULIS in both summer and winter aerosols generally exhibited a higher proportion of humic acid-like substances (V), while having a lower abundance of small-size aromatic proteins I compared to LMW HULIS. These differences are particularly pronounced

in winter aerosols, with the humic acid-like substances accounting for 23% in HMW

HULIS compared to 13% in LMW HULIS, and small-size aromatic proteins I

comprising 9% in HMW HULIS compared to 17% in LMW HULIS (Fig. S5).

Furthermore, the higher HIX values of HMW HULIS (5.64) in comparison to LMW

HULIS (1.94) further support these differences (Table 1). The pronounced BB

emissions and potential NO_2-related oxidation of OA, as evidenced by the presence of

more hotspots (Fig. S1) and higher concentration of NO_2 (Table S1), are likely driving

these marked distinctions between HMW and LMW HULIS in winter aerosols. In

general, these findings imply that the HMW HULIS have a stronger level of

humification and oxidation, while the LMW HULIS appear to be of a simpler nature

and are more likely associated with fresh emissions (e.g., BB).

3.3 Molecular-level insights into MW HULIS

3.3.1. Seasonal variations in the molecular composition of MW HULIS

The molecular-level characteristics of MW HULIS were examined using

negative ESI- HRMS analysis. It is worth noting that the ESI- HRMS could reveal

molecular composition of a subset of organic molecules that are biased ionized in the

negative ESI source rather than representing the entire HULIS composition (He et al.,

2023; Lin et al., 2012). Fig. 3 displays the reconstructed mass spectra of all HULIS

fraction in both summer and winter aerosols. Hundreds of peaks can be observed in

the spectra ranging from m/z 100 to 450 for all samples, with most ions being

abundant within the m/z 150-350 range. These spectrum characteristics are similar to

396   those previously reported for HULIS in ambient aerosols and BB emissions (He et al.,

397   2023; Song et al., 2022; Sun et al., 2021; Wang et al., 2019; Zhang et al., 2021; Zou et

398   al., 2023).
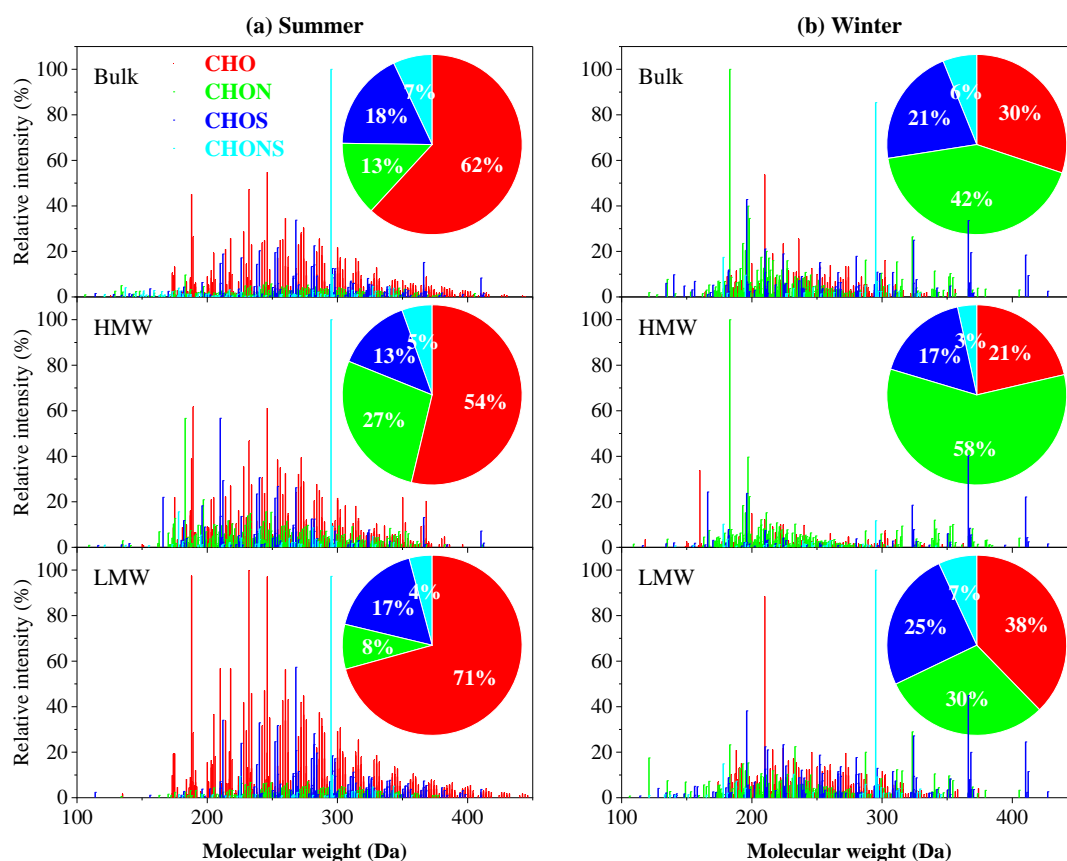
399

400   **Fig. 3.** Mass spectra of bulk and MW HULIS in (a) summer and (b) winter aerosols.

401   The pie charts represent the intensity distributions of four compound categories (CHO,

402   CHON, CHOS, and CHONS).

403

404   As listed in Table 2, the number of assigned formulas within MW HULIS in

405   summer aerosols were 655-672, which was higher than the range of 470-506 observed

406   in winter aerosols. This suggests that the MW HULIS in summer aerosols exhibited

407   greater diversity than those in winter aerosols, mainly due to the stronger SOA

408   formation that enhanced the heterogeneity of HULIS fractions in the summer. The

409   identified formulas were then classified into four groups (i.e., CHO, CHON, CHOS

410   and CHONS) according to their elemental composition. As depicted in pie charts in

411   Fig. 3, summer HULISs are predominantly composed of CHO (54-71%), while winter

412   HULISs feature a high concentration of both CHON (30-58%) and CHO (21-38%).

413   The notably higher content of CHO in summer HULISs are likely due to a wide

414   distribution of biogenic VOC-derived SOAs during the summer season (Li et al., 2022;

415   Sun et al., 2023). CHON content in winter HULISs is generally higher than in

416   summer ones, potentially due to more significant contributions from direct BB, as

417   well as secondary nitrogen-related chemical processes during the winter season (He et

418   al., 2023; Song et al., 2022; Zhang et al., 2021; Zou et al., 2023). This finding is

419   supported by the greater number of fire spots (Fig. S1) and higher concentrations of

420   NO_2 (Table S1) during winter. The higher proportions of CHON compounds in

421   aerosol HULIS typically lead to enhanced light absorption capabilities (He et al., 2023;

422   Song et al., 2022; Zeng et al., 2021). This provides a potential explanation for the

423   higher MAE_{365} values observed in winter HULIS compared to summer HULIS.

424   Additionally, CHOS is more abundant in winter HULISs (17-25%) than in summer

425   aerosols (13-18%). Previous studies have demonstrated that both coal combustion and

426   the oxidation initiated by SO_2 can lead to the generation of larger amounts of

427   S-containing compounds (Song et al., 2018; Song et al., 2022; Zou et al., 2023). This

428   finding suggested that the increased levels of coal combustion and SO_2-related SOAs,

429   as evidenced by higher concentration of SO_2 (Table S1), are significant contributors to

430   the presence of BrC in winter compared to in summer.

Table 2. The average values of intensity-weighted molecular weights (MW), elemental ratios, double bond equivalents (DBE), modified aromaticity index (AI_{mod}) and carbon oxidation state (OS_C) for tentatively identified compounds of the bulk and MW HULIS samples.

		Elemental compositions	Number of formulas	MW_w	H/C_w	O/C_w	N/C_w	S/C_w	O/N_w	O/S_w	OM/OC_w	DBE_w	DBE/C_w	$DBE\text{-}O_w$	$AI_{mod,w}$	$OS_{C,w}$
Summer	BULK	CHO	376	276	1.39	0.59					1.91	4.69	0.39	-2.20	0.15	-0.21
		CHON	270	260	1.35	0.60	0.15		5.52		2.10	4.99	0.50	-1.17	0.27	-0.14
		CHOS	133	278	1.74	0.71		0.11		6.61	2.38	2.21	0.24	-4.41	0.02	-0.33
		CHONS	81	265	1.69	0.59	0.18	0.14	4.98	5.20	2.49	3.38	0.36	-1.95	0.09	-0.52
		Total	860	273	1.47	0.61	0.03	0.03	1.09	1.54	2.06	4.20	0.38	-2.44	0.14	-0.24
	HMW	CHO	270	264	1.41	0.55					1.85	4.51	0.38	-1.70	0.16	-0.32
		CHON	264	248	1.42	0.61	0.14		5.23		2.09	4.44	0.47	-1.33	0.24	-0.20
		CHOS	72	247	1.82	0.75		0.14		5.83	2.53	1.81	0.22	-4.07	0.01	-0.32
		CHONS	39	269	1.55	0.64	0.19	0.15	4.87	5.16	2.60	3.82	0.44	-1.65	0.14	-0.28
		Total	645	258	1.48	0.60	0.05	0.03	1.70	1.07	2.05	4.09	0.39	-1.91	0.16	-0.29
	LMW	CHO	365	275	1.34	0.64					1.97	4.82	0.42	-2.47	0.16	-0.05
		CHON	155	272	1.39	0.66	0.11		6.60		2.12	4.80	0.45	-2.09	0.18	-0.08
		CHOS	120	284	1.71	0.74		0.11		7.05	2.43	2.51	0.25	-4.58	0.02	-0.22
		CHONS	32	322	1.71	0.64	0.11	0.11	6.59	6.63	2.42	3.32	0.30	-3.41	0.06	-0.42
		Total	672	278	1.42	0.66	0.01	0.02	0.80	1.48	2.08	4.36	0.39	-2.84	0.13	-0.10
Winter	BULK	CHO	142	247	1.23	0.48					1.75	5.35	0.47	-0.05	0.32	-0.26
		CHON	194	231	1.24	0.53	0.16		3.96		1.99	5.17	0.57	0.52	0.48	-0.18
		CHOS	79	271	1.93	0.51		0.11		4.97	2.14	1.21	0.14	-3.80	0.04	-0.91
		CHONS	20	271	1.61	0.69	0.16	0.13	5.60	5.90	2.60	3.32	0.40	-2.65	0.09	-0.24
		Total	435	247	1.41	0.52	0.08	0.03	2.02	1.42	1.99	4.27	0.44	-0.77	0.31	-0.37
	HMW	CHO	138	232	1.36	0.47					1.74	4.79	0.41	0.02	0.28	-0.42

	CHON	244	232	1.29	0.53	0.16		3.89		2.01	4.87	0.55	0.23	0.44	-0.23
	CHOS	59	292	2.08	0.40		0.12		4.40	2.04	0.46	0.06	-4.06	0.02	-1.27
	CHONS	29	236	1.74	0.48	0.22	0.20	2.82	3.02	2.57	2.88	0.38	-0.57	0.27	-0.77
	Total	470	242	1.46	0.50	0.10	0.03	2.37	0.85	1.98	4.04	0.43	-0.57	0.33	-0.46
LMW	CHO	176	249	1.23	0.54					1.82	5.25	0.48	-0.65	0.30	-0.15
	CHON	195	239	1.34	0.49	0.16		3.99		1.95	4.88	0.52	0.29	0.45	-0.36
	CHOS	107	280	1.94	0.54		0.10		5.42	2.17	1.20	0.13	-4.25	0.02	-0.85
	CHONS	28	272	1.67	0.69	0.16	0.14	5.89	6.03	2.63	2.99	0.37	-3.15	0.13	-0.29
	Total	506	256	1.47	0.54	0.06	0.04	1.61	1.78	2.01	3.96	0.39	-1.45	0.26	-0.40

433   Table 2 summarizes the intensity-weighted molecular parameters for MW

434   HULIS in both summer and winter aerosols. Evidently, the MWw of summer HULISs

435   are 258-278, which are higher than the corresponding values of 242-256 for winter

436   HULISs. It is noted that these values are considerably smaller than those revealed by

437   HPSEC analysis. This difference could be explained by several factors: (1) ESI-

438   HRMS is based towards relatively small molecules that easily protonated in negative

439   ESI mode (He et al., 2023; Lin et al., 2012); (2) SEC can provide an apparent rather

440   than accurate molecular size of molecules due to the lack of appropriate standards for

441   column calibration (Fan et al., 2023; Wong et al., 2017), and (3) the potential

442   disassembly of larger molecules stabilized by weak forces during electrospray

443   ionization of HRMS (Fan et al., 2021; Phillips et al., 2017). Nevertheless, both HRMS

444   and HPSEC indicate that summer HULISs exhibit larger sizes than winter HULISs.

445   Moreover, summer HULISs exhibit higher O/Cw ranging from 0.60 to 0.66, as well as

446   OS$_{C,w}$ ranging from -0.29 to -0.10, which exceed the respective values of 0.50 to 0.54

447   and -0.46 to -0.37 observed in winter HULISs. Conversely, winter HULISs display

448   higher AI$_{mod,w}$ values (0.26-0.33) than those (0.13-0.16) for summer ones. These

449   findings suggest that summer HULISs are characterized by a high degree of oxidation,

450   while winter HULISs exhibit stronger aromaticity.

451

452   3.3.2. Comparison on molecular composition of HMW and LMW HULIS

453   **CHO compounds.** The CHO compounds are prominent constituents within

454   HULIS fractions, accounting for 54% and 21% in summer and winter HMW HULIS,

455 respectively, whereas these proportions increase to 71% and 38% in LMW HULIS

456 (Fig. 3). It is worth noting that CHO compounds that undergo deprotonation in ESI-

457 mode are likely associated with the presence of carboxyl, carbonyl, alcohol and ester

458 (Lin et al., 2012; Wang et al., 2018). Moreover, CHO compounds in LMW HULIS

459 exhibit a higher oxygenation level compared to HMW HULIS, as evidenced by the

460 higher O/C_w and $OS_{C,w}$ values. As shown in Table 2, the O/C_w for CHO in LMW

461 HULIS are 0.55-0.64, which are higher than 0.47-0.54 observed in HMW HULIS. In

462 contrast, the H/C_w for CHO in HMW HULIS were consistently higher than those in

463 LMW HULIS, with values of 1.41 vs. 1.34 in summer and 1.36 vs. 1.23 in winter

464 (Table 2). This disparity strongly suggests a higher saturation level of CHO

465 compounds within HMW HULIS. This conclusion is further corroborated by the

466 lower DBE_w and $AI_{mod,w}$ observed for CHO in HMW HULIS compared to LMW

467 HULIS (Table 2). It is known that these values serve as estimations of C=C density

468 and aromatic and condensed aromatic structures (Song et al., 2022; Zhang et al.,

469 2021). Taken together, the CHO compounds within HMW HULIS exhibit a more

470 aliphatic nature but lower aromaticity and oxidation levels when compared to those

471 within LMW HULIS.

472 **CHON compounds.** HMW HULIS fractions consist of a higher proportion of

473 CHON compounds compared to LMW HULIS, with proportions of 27% vs. 8% in

474 summer and 58% vs. 30% in winter (Fig. 3). This observation suggests that HMW

475 HULIS contain a higher content of N-containing components. It is noted that the

476 LMW HULIS are generally characterized by higher O/N_w values of 6.60 in summer

477 and 3.99 in winter compared to 5.23 in summer and 3.89 in winter for HMW HULIS.

478 This indicates that the CHON compounds within LMW HULIS are more highly

479 oxidized than those within HMW HULIS. In general, compounds with O/N ≥ 3 are

480 indicative of oxidized N groups such as nitro ($-NO_2$) or nitrooxy ($-ONO_2$), while

481 compounds with O/N < 3 may denote the reduced N-containing functional groups (i.e.,

482 amines) (He et al., 2023; Song et al., 2022; Zeng et al., 2021). In this study, a majority

483 of the CHON compounds, comprising 73-85% in summer and 59-64% in winter,

484 exhibited O/N ≥ 3 in both MW HULIS fractions. This suggests that high

485 concentrations of nitro compounds or organonitrates dominate the CHON compounds

486 (Sun et al., 2023; Wang et al., 2018; Zeng et al., 2021), especially in summer samples,

487 primarily due to the hydroxyl radical oxidation of biogenic or anthropogenic VOC

488 precursors, as well as BB emissions (Song et al., 2022; Sun et al., 2021; Zhang et al.,

489 2021; Zou et al., 2023). Furthermore, the CHON compounds exhibiting O/N ≥ 3 were

490 more abundant in LMW HULIS compared to HMW HULIS, accounting for 85% vs.

491 73% in summer and 64% vs. 59% in winter. In contrast, HMW HULIS contained

492 more CHON compounds with O/N < 3 compared to LMW HULIS. These findings

493 collectively indicate that the CHON within HMW HULIS possess lower content of

494 nitro compounds or organonitrates than LMW HULIS. Based on FTIR analysis (Text

495 S2 and Fig. S6 in SI), it is known that HMW HULIS contain more carboxylic groups

496 than LMW HULIS, which indicate a higher likelihood of HMW HULIS containing

497 more amino acids.

498   **CHOS and CHONS compounds.** In this study, we observed that CHOS

accounted for proportions of 13% to 25% in all MW HULIS fractions, while CHONS

had a lower proportion of 3% to 7% (Fig. 3). Notably, the distribution of CHOS

differed between HMW and LMW HULIS in both season samples. As depicted in Fig.

3, HMW HULIS contained fewer CHOS compounds compared to LMW HULIS, with

proportions of 13% vs. 17% in summer and 17% vs. 25% in winter. This finding

suggests that a greater number of CHOS compounds are incorporated into the LMW

HULIS fractions, which potentially leading to a reduction in the light absorption of

LMW HULIS (Zeng et al., 2021; Zhang et al., 2021). Furthermore, as indicated in

Table 2, both the CHOS and CHONS within LMW HULIS exhibited higher O/Sw

values than HMW HULIS in both seasonal samples. Consequently, the S-containing

compounds within LMW HULIS were characterized by a higher degree of oxidation,

primarily attributed to SO_2-related chemical oxidation process, in comparison to those

in HMW HULIS. Moreover, it was observed that 61% to 92% of CHOS compounds

exhibited O/S > 4, and 3% to 43% of CHONS compounds with O/S > 7 for all MW

HULIS fractions. Among them, HMW HULIS own lower proportions of CHOS with

O/S > 4 and CHONS with O/S > 7 than LMW HULIS, suggesting a reduced presence

of potential organosulfates and nitrooxyorganosulfates within HMW HULIS (Sun et

al., 2023; Wang et al., 2018; Zeng et al., 2021; Zou et al., 2023).

3.3.3. Comparative analysis of unique molecular formulas in HMW and LMW

HULIS

In this study, particular emphasis was placed on the unique molecular formulas

521 within the HMW or LMW HULIS fractions. Fig. 4a, b illustrates the Van Krevelen

522 (VK) diagram depicting the distribution of unique molecular formulas within HMW

523 and LMW HULIS in summer and winter samples. It is evident that a majority of

524 unique formulas within LMW HULIS are concentrated around the origin with O/C >

525 0.5, accounting for 83% in summer and 64% in winter. In contrast, most formulas

526 within HMW HULIS exhibited O/C < 0.5, representing about 58% for both seasonal

527 samples. These findings indicate that the unique molecules within LMW HULIS

528 consist of more polar O-containing organic compounds than those within HMW

529 HULIS.

530
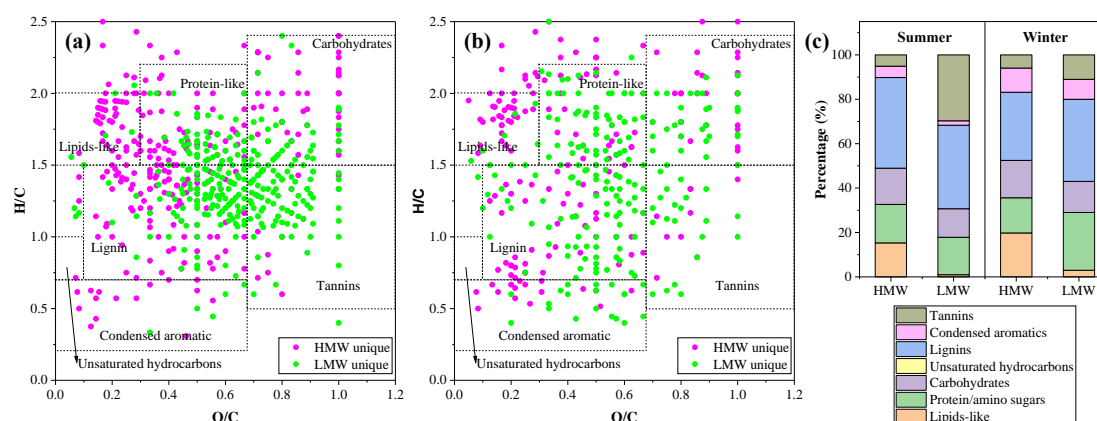
531

532 **Fig. 4.** Van Krevelen diagrams for the unique molecular formulas within HMW and

533 LMW HULIS from (a) summer and (b) winter aerosols. (c) The contributions of

534 major substances classes in unique formulas.

535

536   The molecular formulas are further categorized into seven groups based on

537 previous studies, including lignin-like species, protein/amino sugars, condensed

538 aromatics, tannin-like species, carbohydrate-like species, unsaturated hydrocarbons,

539 and lipid-like species (He et al., 2023; Sun et al., 2021; Sun et al., 2023). The

540 classification rules for these formulas can be found in Table S2. Fig. 4c provides an

541 overview of the relative contributions of the number of unique formulas from each of

542 the seven groups for HMW and LMW HULIS. The results indicate that the dominant

543 substance class in the unique formulas within both MW HULIS are lignin-like species,

544 accounting for proportions of 31-40%. This finding indicates that lignin derivatives

545 are fundamental components in both HMW and LMW HULIS either in summer or

546 winter aerosols. Additionally, there are notable differences in the molecular

547 characteristics of lignin-like species within HMW and LMW HULIS. As listed in

548 Table S3, lignin-like species within HMW HULIS exhibit lower MWw and O/Cw, but

549 higher N/Cw and AImod,w values than those within LMW HULIS in both seasonal

550 samples. These observations suggest that the unique lignin-like substances in HMW

551 HULIS likely contain more N-enriched and highly aromatic species, while those in

552 LMW HULIS tend to concentrate more aliphatic O-containing compounds. These

553 distinctions in composition and characteristics between HMW and LMW HULIS

554 fractions provide valuable insights into their origins and transformations in the

555 atmosphere.

556   Moreover, there are notable variations in the contributions of lipids-like,

557 protein/amino sugars, carbohydrates, condensed aromatics, and tannins species

558 between HMW and LMW HULIS. In general, HMW HULIS have a higher proportion

559 of lipids-like species, carbohydrates and condensed aromatics than LMW HULIS in

560 both summer and winter aerosols. Among these, the most remarkable difference in

561 composition between HMW HULIS and LMW HULIS is seen in lipids-like species,

562 accounting for 15% versus 1% in summer and 20% versus 3% in winter (Fig. 4). As

563 reported in previous studies, lipids-like species primarily originate from biogenic

564 emissions (He et al., 2023; Li et al., 2022; Sun et al., 2021). This suggests that there is

565 a stronger contribution from biogenic emissions to HMW HULIS. Additionally, these

566 species in HMW HULIS were usually characterized by lower DBE_w and slightly

567 lower $OS_{C,w}$ when compared to LMW HULIS (Table S3), indicating they present

568 stronger saturation and fewer oxidized substituents. On the other hand, tannins species

569 contribute a higher proportion to LMW HULIS, constituting 30% in summer and 11%

570 in winter, while comprising only 5%-6% in HMW HULIS in both season aerosols.

571 Tannin-like species are known to consist of various polyphenolic groups containing

572 hydroxyl and carboxylic functional groups (He et al., 2023; Li et al., 2022; Ning et al.,

573 2019; Sun et al., 2021). The slightly lower DBE_w but much higher $DBE\text{-}O_w$ for

574 unique tannin-like species within HMW HULIS were observed compared to LMW

575 HULIS (Table S3), suggesting that the former ones are enriched in more unsaturated

576 O-containing functional groups, particularly carboxylic functional groups.

577

578 3.4. Atmospheric implications

579   This study provides comprehensive comparison between HMW and LMW

580 HULIS regarding their distributions, chemical structures, molecular sizes and

581 compositions. HMW HULIS appear to be larger than LMW HULIS, as evidenced by

582 both ultrafiltration natures and the MW distributions of chromophores analyzed by

583 HPSEC. However, HRMS analysis revealed that the average MWw of identified

584   formulas within HMW HULIS were lower than those of LMW HULIS (Table 2). This

585   discrepancy can likely be attributed to the "assembled structures" that construct the

586   aerosol HULIS, as suggested in many previous studies focusing on HULIS and BrC

587   characterization (Fan et al., 2021; Fan et al., 2023; Phillips et al., 2017; Qin et al.,

588   2022). In fact, the results from EEM-FRI and FTIR analysis support the notion that

589   HMW and LMW HULIS likely consist of potential structures assembled by similar

590   basic fluorophores and functional groups. Based on this theory, HMW HULIS may

591   consist of macromolecular species primarily assembled from small molecules through

592   weak forces (i.e., π–π, van der Waals, hydrophobic, or hydrogen bonds) and/or

593   charge-transfer interactions (Fan et al., 2021; Phillips et al., 2017), which can

594   potentially disassemble during ESI ionization and form low MW molecules.

595   Based on the molecular-level characterization, significant distinctions in

596   properties between HMW HULIS and LMW HULIS become evident. HMW HULIS

597   generally exhibit stronger aromaticity but lower oxidation degree when compared to

598   LMW HULIS. In terms of molecular composition, HMW HULIS contain higher

599   quantities of CHON species but lower quantities of CHO compounds than LMW

600   HULIS. Furthermore, more lipids-like species were identified as unique molecules in

601   HMW HULIS, while more tannin-like species with abundant carboxylic groups were

602   observed as unique molecules in LMW HULIS. Given these pronounced differences

603   between HMW and LMW HULIS, it can be speculated that the higher levels of

604   aromatic structures, greater presence of CHON molecules and the presence of

605   lipids-like species may serve as driving factors in the formation of potential

assembled structures in HMW HULIS. Additionally, it is well-established that CHON can enhance the light absorption of organic aerosols (OA), while CHO species may have the opposite effect, weakening light absorption (He et al., 2023; Song et al., 2022; Wang et al., 2019; Zeng et al., 2021). Therefore, it is reasonable to conclude that HMW HULIS possess stronger light absorbing capability, which is consistent with their larger MAE_{365} values.

Importantly, HMW HULIS contain higher amounts of carboxylic functional groups, reduced nitrogen species (e.g., amines) and aromatic species than LMW HULIS. These functional groups have strong complexation abilities with transition metals (Wang et al., 2021a; Wang et al., 2021b), thus influencing the transformation and chemical behavior of metals. Moreover, the OA-metals complex can potentially enhance the catalytic generation of reactive oxygen species (ROS) in organic aerosols (Win et al., 2018; Zhang et al., 2022a), thereby playing significant roles in adverse health effects of OA. These results reinforce the significance of HMW HULIS in light absorption, metal complexation, and the potential ROS generation ability of aerosol BrC.

4. Conclusions

This study successfully isolated and characterized HMW and LMW HULIS in atmospheric aerosols using the UF-SPE technique, yielding insights into their distribution, optical properties and molecular-level characteristics. Both HMW and LMW HULIS exhibited a continuum of MW distributions ranging from 100 to 20,000

Da. However, HMW HULIS displayed more extensive and intricate MW distributions,

suggesting differences in their sources and formation processes compared to LMW

HULIS. In general, HMW HULIS constituted a higher percentage of TOC and UV254

in aerosols compared to LMW HULIS, indicating the prevalence of hydrophobic and

conjugated aromatic structures in the former. Moreover, HMW HULIS exhibited

higher aromaticity, stronger light absorption abilities, weaker spectra dependence, and

stronger humification and conjugation, compared to LMW HULIS. Interestingly,

HRMS analysis revealed slightly lower MWw values for HMW HULIS than LMW

HULIS, which contradicted the HPSEC results and the nature of UF fractionation.

This finding strongly suggests the possibility of small molecules assembling to form

macromolecules in HMW HULIS. Regarding molecular composition, HMW HULIS

contained a higher proportion of CHON compounds, constituting 27% vs. 8% in

summer and 58% vs. 30% in winter, while LMW HULIS were primarily composed of

CHO compounds, accounting for 71% vs. 54%% in summer and 38% vs. 21% in

winter. Both HMW and LMW HULIS featured lignin-like substances as major unique

molecular formulas, but HMW HULIS exhibited more N-enriched and highly

aromatic species, whereas LMW HULIS contained a higher proportion of polar

O-containing functional groups. Additionally, HMW HULIS included a greater

number of unique lipids-like compounds, while LMW HULIS tend to concentrate

more tannin-like compounds. These observations shed light on the complex nature of

MW HULIS, and their diverse sources and transformations. Future research should

expand the geographical and seasonal coverage to gain a more comprehensive

understanding of the molecular-level characteristics of MW HULIS in various atmospheric environments. Furthermore, exploring additional physicochemical properties of MW HULIS will provide valuable insights into their potential health and environmental implications. Overall, this study offers valuable insights into the molecular-level characteristics of aerosol HULIS, enhancing our understanding of their evolution, sources and potential environmental effects.

Author contribution

Xingjun Fan: Methodology, Supervision, Funding acquisition, Writing-review & editing. **Ao Cheng:** Sampling, Data curation. **Xufang Yu:** Writing-review & editing. **Tao Cao:** Sampling, Investigation. **Dan Chen:** Investigation, Data curation. **Wenchao Ji:** Formal analysis. **Yongbing Cai:** Writing-review & editing. **Fande Meng:** Writing-review & editing. **Jianzhong Song:** Methodology, Writing-review & editing. **Pingan Peng:** Writing-review & editing.

Declaration of Competing Interest

The authors declare that they have no known competing financial interests or personal relationships that could have appeared to influence the work reported in this paper.

Acknowledgments

This study was supported by the Natural Science Foundation of China (42192514, 52100114), the Anhui Provincial Natural Science Foundation (2108085MD140, 2108085QB56), and the State key Laboratory of Organic Geochemistry, GIGCAS (SKLOG202101), Anhui Provincial Key Science Foundation for Outstanding Young

672   Talent (2022AH030145, gxyqZD2021126).

673

674   **References**

675   Bao, M., Zhang, Y.-L., Cao, F., Lin, Y.-C., Hong, Y., Fan, M., Zhang, Y., Yang, X., Xie, F., 2022. Light
676   absorption and source apportionment of water soluble humic-like substances (HULIS) in
677   PM2.5 at Nanjing, China. Environmental Research 206, 112554.
678   Birdwell, J.E., Valsaraj, K.T., 2010. Characterization of dissolved organic matter in fogwater by
679   excitation–emission matrix fluorescence spectroscopy. Atmos. Environ. 44, 3246-3253.
680   Cao, T., Li, M., Xu, C., Song, J., Fan, X., Li, J., Jia, W., Peng, P., 2022. Technical note: Identification of
681   chemical composition and source of fluorescent components in atmospheric
682   water-soluble brown carbon by excitation-emission matrix with parallel factor analysis:
683   Potential limitation and application. Atmos. Chem. Phys. Discuss. 2022, 1-41.
684   Cao, T., Li, M., Zou, C., Fan, X., Song, J., Jia, W., Yu, C., Yu, Z., Peng, P., 2021. Chemical composition,
685   optical properties, and oxidative potential of water- and methanol-soluble organic
686   compounds emitted from the combustion of biomass materials and coal. Atmos. Chem.
687   Phys. 21, 13187-13205.
688   Chen, J., Wu, Z.J., Zhao, X., Wang, Y.J., Chen, J.C., Qiu, Y.T., Zong, T.M., Chen, H.X., Wang, B.B., Lin,
689   P., Liu, W., Guo, S., Yao, M.S., Zeng, L.M., Wex, H., Liu, X., Hu, M., Li, S.M., 2021a.
690   Atmospheric Humic-Like Substances (HULIS) Act as Ice Active Entities. Geophysical
691   Research Letters 48, e2021GL092443.
692   Chen, Q., Hua, X., Dyussenova, A., 2021b. Evolution of the chromophore aerosols and its driving
693   factors in summertime Xi'an, Northwest China. Chemosphere 281, 130838.
694   Chen, W., Westerhoff, P., Leenheer, J.A., Booksh, K., 2003. Fluorescence Excitation-Emission
695   Matrix Regional Integration to Quantify Spectra for Dissolved Organic Matter. Environ.
696   Sci. Technol. 37, 5701-5710.
697   Di Lorenzo, R.A., Place, B.K., VandenBoer, T.C., Young, C.J., 2018. Composition of Size-Resolved
698   Aged Boreal Fire Aerosols: Brown Carbon, Biomass Burning Tracers, and Reduced
699   Nitrogen. ACS Earth and Space Chemistry 2, 278-285.
700   Di Lorenzo, R.A., Washenfelder, R.A., Attwood, A.R., Guo, H., Xu, L., Ng, N.L., Weber, R.J., Baumann,
701   K., Edgerton, E., Young, C.J., 2017. Molecular-Size-Separated Brown Carbon Absorption
702   for Biomass-Burning Aerosol at Multiple Field Sites. Environ. Sci. Technol. 51, 3128-3137.
703   Dinar, E., Taraniuk, I., Graber, E.R., Anttila, T., Mentel, T.F., Rudich, Y., 2007. Hygroscopic growth of
704   atmospheric and model humic-like substances. J.Geophys. Res. 112.
705   Fan, X., Cai, F., Xu, C., Yu, X., Wang, Y., Xiao, X., Ji, W., Cao, T., Song, J., Peng, P.a., 2021. Molecular
706   weight-dependent abundance, absorption, and fluorescence characteristics of
707   water-soluble organic matter in atmospheric aerosols. Atmos. Environ. 247.
708   Fan, X., Cao, T., Yu, X., Wang, Y., Xiao, X., Li, F., Xie, Y., Ji, W., Song, J., Peng, P., 2020. The
709   evolutionary behavior of chromophoric brown carbon during ozone aging of fine
710   particles from biomass burning. Atmos. Chem. Phys. 20, 4593-4605.
711   Fan, X., Cheng, A., Chen, D., Cao, T., Ji, W., Song, J., Peng, P., 2023. Investigating the molecular
712   weight distribution of atmospheric water-soluble brown carbon using high-performance

size exclusion chromatography coupled with diode array and fluorescence detectors. Chemosphere 338, 139517.

Fan, X., Li, M., Cao, T., Cheng, C., Li, F., Xie, Y., Wei, S., Song, J., Peng, P.a., 2018. Optical properties and oxidative potential of water- and alkaline-soluble brown carbon in smoke particles emitted from laboratory simulated biomass burning. Atmos. Environ. 194, 48-57.

Fan, X., Song, J., Peng, P., 2013. Comparative study for separation of atmospheric humic-like substance (HULIS) by ENVI-18, HLB, XAD-8 and DEAE sorbents: elemental composition, FT-IR, 1H NMR and off-line thermochemolysis with tetramethylammonium hydroxide (TMAH). Chemosphere 93, 1710-1719.

Fan, X., Song, J., Peng, P.a., 2016a. Temporal variations of the abundance and optical properties of water soluble Humic-Like Substances (HULIS) in PM2.5 at Guangzhou, China. Atmos. Res. 172–173, 8-15.

Fan, X., Wei, S., Zhu, M., Song, J., Peng, P., 2016b. Comprehensive characterization of humic-like substances in smoke PM2.5 emitted from the combustion of biomass materials and fossil fuels. Atmos. Chem. Phys. 16, 13321-13340.

Fan, X., Yu, X., Wang, Y., Xiao, X., Li, F., Xie, Y., Wei, S., Song, J., Peng, P.a., 2019. The aging behaviors of chromophoric biomass burning brown carbon during dark aqueous hydroxyl radical oxidation processes in laboratory studies. Atmos. Environ. 205, 9-18.

Fan, X.J., Song, J.Z., Peng, P.A., 2012. Comparison of isolation and quantification methods to measure humic-like substances (HULIS) in atmospheric particles. Atmos. Environ. 60, 366-374.

Graber, E.R., Rudich, Y., 2006. Atmospheric HULIS: How humic-like are they? A comprehensive and critical review. Atmos. Chem. Phys. 6, 729-753.

He, T., Wu, Y., Wang, D., Cai, J., Song, J., Yu, Z., Zeng, X., Peng, P.a., 2023. Molecular compositions and optical properties of water-soluble brown carbon during the autumn and winter in Guangzhou, China. Atmos. Environ. 296, 119573.

Huo, Y., Wang, Y., Qi, W., Jiang, M., Li, M., 2021. Comprehensive characterizations of HULIS in fresh and secondary emissions of crop straw burning. Atmos. Environ. 248, 118220.

Kawasaki, N., Matsushige, K., Komatsu, K., Kohzu, A., Nara, F.W., Ogishi, F., Yahata, M., Mikami, H., Goto, T., Imai, A., 2011. Fast and precise method for HPLC–size exclusion chromatography with UV and TOC (NDIR) detection: Importance of multiple detectors to evaluate the characteristics of dissolved organic matter. Water Res. 45, 6240-6248.

Kumar, V., Goel, A., Rajput, P., 2017. Compositional and surface characterization of HULIS by UV-Vis, FTIR, NMR and XPS: Wintertime study in Northern India. Atmos. Environ. 164, 468-475.

Li, X., Yu, F., Cao, J., Fu, P., Hua, X., Chen, Q., Li, J., Guan, D., Tripathee, L., Chen, Q., Wang, Y., 2022. Chromophoric dissolved organic carbon cycle and its molecular compositions and optical properties in precipitation in the Guanzhong basin, China. Sci. Total Environ. 814, 152775.

Lin, P., Rincon, A.G., Kalberer, M., Yu, J.Z., 2012. Elemental composition of HULIS in the Pearl River Delta Region, China: results inferred from positive and negative electrospray high resolution mass spectrometric data. Environ. Sci. Technol. 46, 7454-7462.

Ma, Y., Cheng, Y., Qiu, X., Cao, G., Kuang, B., Yu, J.Z., Hu, D., 2019. Optical properties, source apportionment and redox activity of humic-like substances (HULIS) in airborne fine

757 particulates in Hong Kong. Environmental Pollution 255, 113087.

758 Mukherjee, A., Dey, S., Rana, A., Jia, S., Banerjee, S., Sarkar, S., 2020. Sources and atmospheric
759 processing of brown carbon and HULIS in the Indo-Gangetic Plain: Insights from
760 compositional analysis. Environmental Pollution 267, 115440.

761 Ning, C., Gao, Y., Zhang, H., Yu, H., Wang, L., Geng, N., Cao, R., Chen, J., 2019. Molecular
762 characterization of dissolved organic matters in winter atmospheric fine particulate
763 matters (PM2.5) from a coastal city of northeast China. Sci. Total Environ. 689, 312-321.

764 Phillips, S.M., Bellcross, A.D., Smith, G.D., 2017. Light Absorption by Brown Carbon in the
765 Southeastern United States is pH-dependent. Environ. Sci. Technol. 51, 6782-6790.

766 Piccolo, A., 2002. The supramolecular structure of humic substances: A novel understanding of
767 humus chemistry and implications in soil science, Advances in Agronomy. Academic
768 Press, pp. 57-134.

769 Qin, J., Zhang, L., Qin, Y., Shi, S., Li, J., Gao, Y., Tan, J., Wang, X., 2022. pH-Dependent Chemical
770 Transformations of Humic-Like Substances and Further Cognitions Revealed by Optical
771 Methods. Environ. Sci. Technol. 56, 7578-7587.

772 Qin, J., Zhang, L., Zhou, X., Duan, J., Mu, S., Xiao, K., Hu, J., Tan, J., 2018. Fluorescence
773 fingerprinting properties for exploring water-soluble organic compounds in PM 2.5 in an
774 industrial city of northwest China. Atmos. Environ. 184, 203-211.

775 Santos, P.S.M., Otero, M., Duarte, R.M.B.O., Duarte, A.C., 2009. Spectroscopic characterization of
776 dissolved organic matter isolated from rainwater. Chemosphere 74, 1053-1061.

777 Santos, P.S.M., Santos, E.B.H., Duarte, A.C., 2012. First spectroscopic study on the structural
778 features of dissolved organic matter isolated from rainwater in different seasons. Sci.
779 Total Environ. 426, 172-179.

780 Song, J., Li, M., Jiang, B., Wei, S., Fan, X., Peng, P., 2018. Molecular Characterization of
781 Water-Soluble Humic like Substances in Smoke Particles Emitted from Combustion of
782 Biomass Materials and Coal Using Ultrahigh-Resolution Electrospray Ionization Fourier
783 Transform Ion Cyclotron Resonance Mass Spectrometry. Environ. Sci. Technol. 52,
784 2575-2585.

785 Song, J., Li, M., Zou, C., Cao, T., Fan, X., Jiang, B., Yu, Z., Jia, W., Peng, P.a., 2022. Molecular
786 Characterization of Nitrogen-Containing Compounds in Humic-like Substances Emitted
787 from Biomass Burning and Coal Combustion. Environ. Sci. Technol. 56, 119-130.

788 Song, J.Z., Huang, W.L., Peng, P.A., Xiao, B.H., Ma, Y.J., 2010. Humic Acid Molecular Weight
789 Estimation by High-Performance Size-Exclusion Chromatography with Ultraviolet
790 Absorbance Detection and Refractive Index Detection. Soil. Sci. Soc. Am. J. 74,
791 2013-2020.

792 Sun, H., Li, X., Zhu, C., Huo, Y., Zhu, Z., Wei, Y., Yao, L., Xiao, H., Chen, J., 2021. Molecular
793 composition and optical property of humic-like substances (HULIS) in winter-time PM2.5
794 in the rural area of North China Plain. Atmos. Environ. 252, 118316.

795 Sun, H., Wu, Z., Kang, X., Zhu, C., Yu, L., Li, R., Lin, Z., Chen, J., 2023. Molecular characterization of
796 humic-like substances (HULIS) in atmospheric particles (PM2.5) in offshore Eastern China
797 Sea (OECS) using solid-phase extraction coupled with ESI FT-ICR MS. Atmos. Environ.
798 294, 119523.

799 Wang, K., Zhang, Y., Huang, R.-J., Cao, J., Hoffmann, T., 2018. UHPLC-Orbitrap mass
800 spectrometric characterization of organic aerosol from a central European city (Mainz,

801   Germany) and a Chinese megacity (Beijing). Atmos. Environ. 189, 22‑29.

802 Wang, X., Qin, Y., Qin, J., Long, X., Qi, T., Chen, R., Xiao, K., Tan, J., 2021a. Spectroscopic insight
803   into the pH-dependent interactions between atmospheric heavy metals (Cu and Zn) and
804   water-soluble organic compounds in PM2.5. Sci. Total Environ. 767, 145261.

805 Wang, X.B., Qin, Y.Y., Qin, J.J., Yang, Y.R., Qi, T., Chen, R.Z., Tan, J.H., Xiao, K., 2021b. The
806   interaction laws of atmospheric heavy metal ions and water-soluble organic compounds
807   in PM2.5 based on the excitation-emission matrix fluorescence spectroscopy. Journal of
808   Hazardous Materials 402, 8.

809 Wang, Y., Hu, M., Lin, P., Tan, T., Li, M., Xu, N., Zheng, J., Du, Z., Qin, Y., Wu, Y., Lu, S., Song, Y., Wu,
810   Z., Guo, S., Zeng, L., Huang, X., He, L., 2019. Enhancement in Particulate Organic Nitrogen
811   and Light Absorption of Humic-Like Substances over Tibetan Plateau Due to
812   Long-Range Transported Biomass Burning Emissions. Environ. Sci. Technol. 53,
813   14222‑14232.

814 Win, M.S., Tian, Z., Zhao, H., Xiao, K., Peng, J., Shang, Y., Wu, M., Xiu, G., Lu, S., Yonemochi, S.,
815   Wang, Q., 2018. Atmospheric HULIS and its ability to mediate the reactive oxygen
816   species (ROS): A review. J Environ Sci (China) 71, 13-31.

817 Wong, J.P.S., Nenes, A., Weber, R.J., 2017. Changes in Light Absorptivity of Molecular Weight
818   Separated Brown Carbon Due to Photolytic Aging. Environ. Sci. Technol. 51, 8414-8421.

819 Wong, J.P.S., Tsagkaraki, M., Tsiodra, I., Mihalopoulos, N., Violaki, K., Kanakidou, M., Sciare, J.,
820   Nenes, A., Weber, R.J., 2019. Atmospheric evolution of molecular-weight-separated
821   brown carbon from biomass burning. Atmos. Chem. Phys. 19, 7319-7334.

822 Wu, G., Fu, P., Ram, K., Song, J., Chen, Q., Kawamura, K., Wan, X., Kang, S., Wang, X., Laskin, A.,
823   Cong, Z., 2021. Fluorescence characteristics of water-soluble organic carbon in
824   atmospheric aerosol☆. Environmental Pollution 268, 115906.

825 Wu, G., Wan, X., Gao, S., Fu, P., Yin, Y., Li, G., Zhang, G., Kang, S., Ram, K., Cong, Z., 2018.
826   Humic-Like Substances (HULIS) in Aerosols of Central Tibetan Plateau (Nam Co, 4730 m
827   asl): Abundance, Light Absorption Properties, and Sources. Environ. Sci. Technol. 52,
828   7203-7211.

829 Wu, G., Wan, X., Ram, K., Li, P., Liu, B., Yin, Y., Fu, P., Loewen, M., Gao, S., Kang, S., Kawamura, K.,
830   Wang, Y., Cong, Z., 2020. Light absorption, fluorescence properties and sources of brown
831   carbon aerosols in the Southeast Tibetan Plateau. Environmental Pollution 257, 113616.

832 Yuan, W., Huang, R.-J., Yang, L., Ni, H., Wang, T., Cao, W., Duan, J., Guo, J., Huang, H., Hoffmann,
833   T., 2021. Concentrations, optical properties and sources of humic-like substances (HULIS)
834   in fine particulate matter in Xi'an, Northwest China. Sci. Total Environ. 789, 147902.

835 Zeng, Y., Ning, Y., Shen, Z., Zhang, L., Zhang, T., Lei, Y., Zhang, Q., Li, G., Xu, H., Ho, S.S.H., Cao, J.,
836   2021. The Roles of N, S, and O in Molecular Absorption Features of Brown Carbon in
837   PM2.5 in a Typical Semi-Arid Megacity in Northwestern China. Journal of Geophysical
838   Research: Atmospheres 126, e2021JD034791.

839 Zhang, T., Huang, S., Wang, D., Sun, J., Zhang, Q., Xu, H., Hang Ho, S.S., Cao, J., Shen, Z., 2022a.
840   Seasonal and diurnal variation of PM2.5 HULIS over Xi'an in Northwest China: Optical
841   properties, chemical functional group, and relationship with reactive oxygen species
842   (ROS). Atmos. Environ. 268, 118782.

843 Zhang, T., Shen, Z., Huang, S., Lei, Y., Zeng, Y., Sun, J., Zhang, Q., Ho, S.S.H., Xu, H., Cao, J., 2022b.
844   Optical properties, molecular characterizations, and oxidative potentials of different

845   polarity levels of water-soluble organic matters in winter PM2.5 in six China's megacities.
846   Sci. Total Environ. 853, 158600.

847   Zhang, T., Shen, Z., Zeng, Y., Cheng, C., Wang, D., Zhang, Q., Lei, Y., Zhang, Y., Sun, J., Xu, H., Ho,
848   S.S.H., Cao, J., 2021. Light absorption properties and molecular profiles of HULIS in PM2.5
849   emitted from biomass burning in traditional "Heated Kang" in Northwest China. Sci. Total
850   Environ. 776, 146014.

851   Zhang, T., Shen, Z., Zhang, L., Tang, Z., Zhang, Q., Chen, Q., Lei, Y., Zeng, Y., Xu, H., Cao, J., 2020.
852   PM2.5 Humic-like substances over Xi'an, China: Optical properties, chemical functional
853   group, and source identification. Atmos. Res. 234, 104784.

854   Zhang, W., Li, L., Wang, D., Wang, R., Yu, S., Gao, N., 2022c. Characterizing dissolved organic
855   matter in aquatic environments by size exclusion chromatography coupled with multiple
856   detectors. Anal. Chim. Acta 1191, 339358.

857   Zheng, G.J., He, K.B., Duan, F.K., Cheng, Y., Ma, Y.L., 2013. Measurement of humic-like substances
858   in aerosols: A review. Environmental Pollution 181, 301-314.

859   Zou, C., Cao, T., Li, M., Song, J., Jiang, B., Jia, W., Li, J., Ding, X., Yu, Z., Zhang, G., Peng, P.a., 2023.
860   Measurement report: Changes in light absorption and molecular composition of
861   water-soluble humic-like substances during a winter haze bloom-decay process in
862   Guangzhou, China. Atmos. Chem. Phys. 23, 963-979.

863   Zou, C., Li, M., Cao, T., Zhu, M., Fan, X., Peng, S., Song, J., Jiang, B., Jia, W., Yu, C., Song, H., Yu, Z.,
864   Li, J., Zhang, G., Peng, P.a., 2020. Comparison of solid phase extraction methods for the
865   measurement of humic-like substances (HULIS) in atmospheric particles. Atmos. Environ.
866   225, 117370.

867

868